Available online at www.sciencedirect.com

ScienceDirect

Mendeleev Commun., 2020, **30**, 126–128

Mendeleev Communications

Effect of WO_3 particle size on the type and concentration of surface oxygen

Lili Yang, Artem V. Marikutsa,* Marina N. Rumyantseva and Alexander M. Gaskov

Department of Chemistry, M. V. Lomonosov Moscow State University, 119991 Moscow, Russian Federation. Fax: +7 495 932 8846; e-mail: artem.marikutsa@gmail.com

DOI: 10.1016/j.mencom.2020.01.043

X-ray photoelectron spectroscopy and electric conduction measurements performed for nanocrystalline WO_3 revealed that the ratio of surface-to-bulk oxygen decreased, and the predominant type of chemisorbed oxygen changed from molecular O_2^- to atomic O^- and O^{2-} species with the increment of WO_3 particle size.

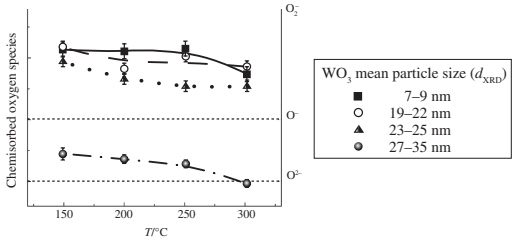

Keywords: tungsten oxide, nanoparticles, chemisorbed oxygen, surface sites, semiconductor oxide.

Tungsten oxide is an *n*-type semiconductor possessing the bandgap width of 2.6 eV.[1] Nanostructures based on WO_3 are of interest in gas sensing, catalysis, and photocatalysis.[1–3] The gas sensors utilizing nanocrystalline WO_3 are promising for the detection of toxic gases (nitrogen oxides, NH_3, H_2S, *etc.*) and exhaled breath analysis.[4–8] An oxygen chemisorption on the surfaces of *n*-type metal oxide semiconductors plays the key role in gas sensing mechanisms.[9] Although the chemisorbed oxygen is often considered in the studies on tungsten oxide-based sensors,[6,10–12] the types and amounts of surface oxygen species and the effect of WO_3 microstructure on the chemisorbed oxygen have not yet been established.

In the present work, nanocrystalline WO_3 incorporating particles of different sizes and specific surface area (SSA) was synthesized. The relative amounts of surface-to-bulk oxygen anions were quantified by X-ray photoelectron spectroscopy (XPS). Chemisorbed oxygen species were detected by the resistance measurements under controlled oxygen partial pressure. The WO_3 samples were obtained *via* a deposition of tungstic acid from an aqueous solution of ammonium paratungstate, followed by an annealing at different temperatures in the range of 300–800 °C.† According to X-ray diffraction (XRD) data, all the samples consisted of the monoclinic γ-WO_3 (ICDD #43-1035). Mean particle size (d_{XRD}) and SSA were correspondingly increased and decreased with raising the annealing temperature of WO_3 (Figure 1). XPS signals from the W 4*f* and O 1*s* levels (Figures S1 and S2, in Online Supplementary Materials) were recorded for the WO_3 samples containing particles of different sizes.‡ Tungsten was found mainly in the W^{6+} state with a small fraction of the W^{5+} state. The occurrence of W^{5+} in WO_3 agrees with the intrinsic oxygen deficiency that can be expressed as $WO_{3-\delta}$.[1] Oxygen was observed roughly in two states: the lattice anions O^{2-}_{bulk} with the binding energy of 530.1 eV and the surface oxygen species O_{surf} with the binding energy of 530.7–531.0 eV. The oxidation state of surface oxygen cannot be unambiguously deconvoluted from the XPS signals (see Figure S2). The broad peak of O_{surf} may be a sum of overlapping peaks of different oxidation states of oxygen, such as surface anions O^{2-}, chemisorbed oxygen (O_2^-, O^-, and O^{2-}), and OH groups. The positions of XPS peaks for O_{surf} coincided

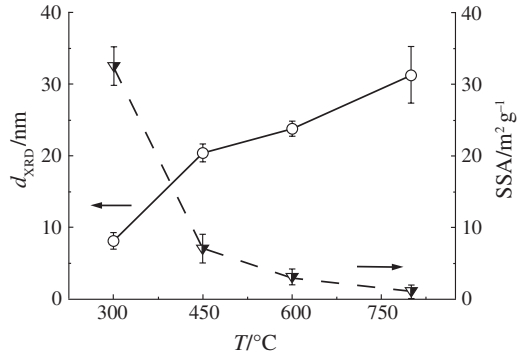

Figure 1 Dependences of mean particle size and specific surface area of the nanocrystalline WO_3 samples on the annealing temperature.

† Ammonium paratungstate (APT, Sigma-Aldrich, >99% pure) was dissolved in distilled water to obtain 16 mM solution. Nitric acid (7.8 M) was added dropwise to the stirred APT solution at 80 °C to reach the resulting concentrations of 10 mM and 3 M for APT and HNO_3, respectively. This mixture was stirred at 80 °C for 30 min and cooled to room temperature within 1 h. The precipitate of tungstic acid was centrifuged, washed by deionized H_2O, and dried at 80 °C. The dried residual was separated into four parts, which were annealed for 24 h at different temperatures: 300, 450, 600 and 800 °C.

‡ X-ray powder diffraction was measured with a DRON-3M diffractometer, CuKα radiation (0.154 nm). Specific surface area was evaluated by nitrogen adsorption according to the Brunauer–Emmett–Teller (BET) model using a Chemisorb 2750 (Micromeritics) instrument. DC-resistance was measured by a PC-controlled electrometer equipped with a flow chamber. Powders were dispersed in terpineol, and the paste was deposited onto alumina substrates with Pt contacts (0.3×0.2 mm, gap of 0.2 mm) and Pt-heaters. The binder was removed at 200 °C; the size of thick films was 1×0.5 mm^2, and their thickness was about 10 mm. Resistance was measured at a voltage of 1.3 V under Ar flow (99.999% pure, 100 ml min^{-1}) mixed with pure air from a generator of pure air (model '1,2-3,5', Khimelectronika). Oxygen partial pressure was varied in the range of 0.00–0.20 bar with the step of 0.04 bar. Temperature of measurements was varied in the range of 150–300 °C with the step of 50 °C.

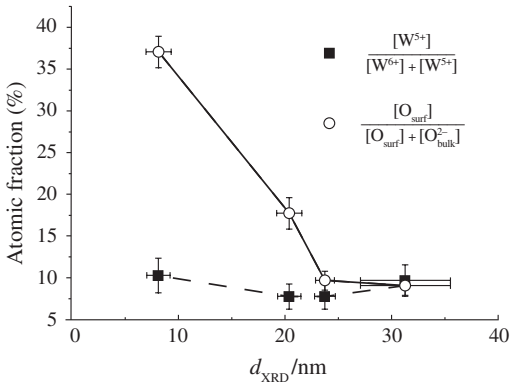

Figure 2 Atomic fractions of W^{5+} in the total tungsten content and those of surface oxygen species (O_{surf}) in the total oxygen content in nanocrystalline WO_3 as a function of mean particle size estimated by XRD.

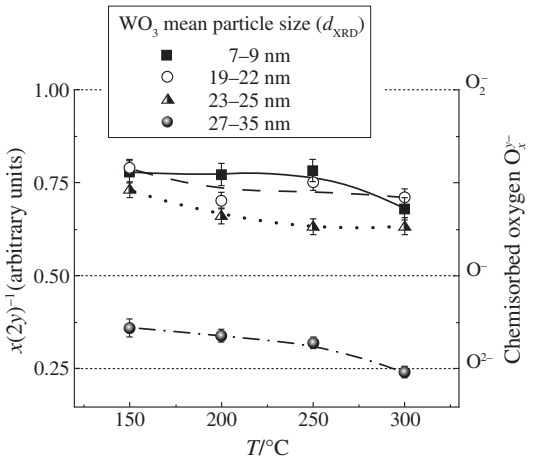

Figure 3 The temperature dependence of parameter $x/2y$ and the corresponding type of chemisorbed oxygen O_x^{y-} on the surface of nanocrystalline WO_3 with different mean particle sizes estimated by XRD.

among the examined WO_3 samples (see Figure S2), which means an absence of any XPS-detectable effect of the particle size of WO_3 on the nature of surface oxygen species. The atomic ratios of the W and O elements in different states were estimated from the areas of XPS signals. The fraction of W^{5+} was 8–10 % from the total W content, irrespective of the particle size of WO_3 (Figure 2). The fraction of surface oxygen (O_{surf}) in its total content reduced as the particle size of WO_3 increased (see Figure 2). It can be explained by the decrease in atomic surface-to-bulk ratio with the increment of the particle size. The decreased O_2 chemisorption on the surface of WO_3 with lower SSA can also be the reason for the reduction of surface oxygen fraction.

The type of chemisorbed oxygen species on WO_3 was estimated from the dependences of electric conductance on oxygen partial pressure. The estimation was performed according to the model reported previously.[13,14] The chemisorption of O_2 results in trapping electrons on the surface of an *n*-type semiconductor:

$$x/2\ O_{2(gas)} + y\ e^- = O^{y-}_{x(ads)}. \quad (1)$$

Concentration of electrons on the grains surface (n_s) determines the electric conductance. According to mass action law, it depends on oxygen partial pressure $p(O_2)$ and the type of chemisorbed species $O^{y-}_{x(ads)}$ (*i.e.*, parameters x and y) according to the following equation:

$$n_s^y = k_{des}/k_{ads}\ S\ [p(O_2)]^{-x/2}, \quad (2)$$

where k_{des} and k_{ads} are the rate constants of desorption and adsorption, respectively, and S is the concentration of adsorption sites occupied by chemisorbed oxygen. The latter is a function of n_s and depends on the particle size (d) in relation to the thickness (L) of the depletion layer formed within the semiconductor due to the oxygen chemisorption. For a porous nanocrystalline layer consisting of the small particles with $d < 2L$, *i.e.* in the case of full depletion of the semiconductor grains by electrons (the case of flat bands), the conductance (σ) depends on the oxygen partial pressure, according to equation (3). If oxygen is chemisorbed on the larger particles ($d > 2L$), *i.e.* in the case of band bending due to surface potential barrier formation, the conductance σ depends on the oxygen partial pressure, according to equation (4).[13,14]

$$\lg\sigma - \lg(1 - \sigma/\sigma_0) = \text{constant} - x/2y\ \lg[p(O_2)] \quad (\text{small particles}, d < 2L), \quad (3)$$

$$\lg\sigma - \tfrac{1}{2}\lg[\ln(\sigma_0/\sigma)] = \text{constant} - x/2y\ \lg[p(O_2)] \quad (\text{large particles}, d > 2L), \quad (4)$$

where σ is the conductance in presence of oxygen, σ_0 is the conductance under inert atmosphere (Ar). The threshold size of WO_3 particles, $d = 2L = 33$ nm, was previously reported.[17] Slope $x/2y$ shows the type of chemisorbed oxygen. For example, three types of oxygen species chemisorbed on *n*-type semiconductor (SnO_2) are known:[15] O_2^- ($x/2y = 1$) at 100–160 °C, O^- ($x/2y = 0.5$) at 200–350 °C, and O^{2-} ($x/2y = 0.25$) at temperatures above 350 °C.

The dynamic DC-resistance of the samples exposed to gas flow of Ar–air with variable oxygen percentage (Figure S3) and the logarithmic dependences of steady conductance values on oxygen partial pressure (Figure S4) were plotted. The logarithmic dependences of conductance on $p(O_2)$ for the WO_3 samples with the mean particle size d_{XRD} = 7–25 nm (estimated by XRD) are linear in the coordinates corresponding to equation (3) [Figure S3(*b*)], and the dependences for the sample with the mean particle size d_{XRD} = 27–35 nm are linear in the coordinates of equation (4) [Figure S4(*b*)]. Figure 3 shows the $x/2y$ parameter estimated from the slopes of these dependences and corresponding to the definite types of chemisorbed oxygen. For the samples with the mean particle sizes below 22 nm, the parameters are close to $x/2y \approx 0.75$. Hence, oxygen is chemisorbed equally in the forms of the molecular O_2^- and atomic O^- species. For the samples of WO_3 with larger nanocrystals, the parameter $x/2y$ decreased to 0.70–0.60 (d_{XRD} = 23–25 nm) and 0.40–0.25 (d_{XRD} = 27–35 nm) (see Figure 3). Thus, the predominant type of chemisorbed oxygen changes to atomic O^- and O^{2-} species upon increasing the particle size of WO_3. The similar influence of particle size on the predominant type of chemisorbed oxygen was reported in literature for other *n*-type metal oxides (SnO_2 and In_2O_3).[14] It was rationalized in the other work:[16] the grains of diameter (d) less than double thickness of the depletion layer (L) are fully depleted of electrons because of trapping at surface states. The Fermi level is shifted above the energy states of O_2^-, which makes molecular ionosorption energetically favorable on the nanoparticles with $d < 2L$:

$$O_{2(gas)} + e^-_{(bulk)} = O^-_{2(ads)}. \quad (5)$$

In the larger particles ($d > 2L$), the Fermi level is below the energy level of O^-_2, but above the levels of O^- and O^{2-}. It makes the molecular ionosorbates instable and facilitates their transition into atomic species:

$$O^-_{2(ads)} + e^-_{(bulk)} = 2\ O^-_{(ads)}, \quad (6)$$

$$O^-_{(ads)} + e^-_{(bulk)} = O^{2-}_{(ads)}. \quad (7)$$

Such an explanation of the effect of Fermi level position on the type of chemisorbed oxygen species is in agreement with our observation for nanocrystalline WO_3. As one can conclude from Figure 3, the samples of WO_3 with particle sizes below the threshold size of $d < 2L = 33$ nm are prone for the chemisorption of molecular O_2^- and atomic O^- species according to equations (5) and (6). Oxygen is chemisorbed mostly as the atomic species [equations (6) and (7)] on the WO_3 surface with the particle size reaching 35 nm, *i.e.* exceeding the double depletion layer. Noteworthy, no change of the type of oxygen surface species was inferred from the XPS spectra of the WO_3 samples with different particle size (see Figure S2). It can be explained by different measurement conditions: the XPS spectra were recorded at room temperature under ultra-high vacuum, while the conductance measurements were performed for the temperatures of 150–300 °C and ambient pressure.

The predominant type of chemisorbed oxygen species on the WO_3 samples was dependent on temperature (Figure 3). For WO_3 with $d_{XRD} < 25$ nm, an increasing impact of the atomic O^- species, in contrast to the molecular ones O_2^-, was observed with the increase of temperature from 150 to 300 °C. Such an effect of temperature on the predominant route of oxygen chemisorption is typical of *n*-type semiconducting metal oxides.[15] It is explained by the fact that the dissociation of molecular oxygen and the ionization of atomic species to the O^- and further to the O^{2-} ones require a thermal activation.[15] For WO_3 with $d_{XRD} = 27–35$ nm, the predominant type of chemisorbed oxygen changed from the single-ionized O^- to the double-ionized O^{2-} species upon increasing temperature from 150 to 300 °C (see Figure 3).

In conclusion, the amount of surface oxygen relative to bulk oxygen species decreases, as the particle size of WO_3 increases within the range of 7–35 nm. Oxygen is chemisorbed predominantly in the forms of O_2^- and O^- species on the surface of nanocrystalline WO_3 with particle size below 22 nm. The obtained results are valuable for the design and applications of nanocrystalline WO_3-based materials in gas sensors, since the knowledge of chemisorbed oxygen species on the WO_3 surface is necessary for understanding the sensing mechanisms and for the control of sensing behavior depending on the particle size of semiconductor and temperature.

This work was supported by the Russian Science Foundation (grant no. 19-13-00245).

Online Supplementary Materials

Supplementary data associated with this article can be found in the online version at doi: 10.1016/j.mencom.2020.01.043.

References

1 Z.-F. Huang, J. Song, L. Pan, X. Zhang, L. Wan and J.-J. Zou, *Adv. Mater.*, 2015, **27**, 5309.
2 H. Long, W. Zeng and H. Zhang, *J. Mater. Sci.: Mater. Electron.*, 2015, **26**, 4698.
3 J. Kukkola, J. Maklin, N. Halonen, T. Kyllönen, G. Tóh, M. Szabó, A. Shchukarev, J.-P. Mikkola, H. Jantunen and K. Kordás, *Sens. Actuators, B*, 2011, **153**, 293.
4 B. Timmer, W. Olthuis and A. van den Berg, *Sens. Actuators, B*, 2005, **107**, 666.
5 A. A. Tomchenko, V. V. Khatko and I. L. Emelianov, *Sens. Actuators, B*, 1998, **46**, 8.
6 H. Xia, Y. Wang, F. Kong, S. Wang, B. Zhu, X. Guo, J. Zhang, Y. Wang and S. Wu, *Sens. Actuators, B*, 2008, **134**, 133.
7 A. Staerz, U. Weimar and N. Barsan, *Sensors*, 2016, **16**, 1815.
8 M. Righettoni, A. Tricoli, S. Gass, A. Schmid, A. Amann and S. E. Pratsinis, *Anal. Chim. Acta*, 2012, **738**, 69.
9 G. N. Gerasimov, V. F. Gromov, O. J. Ilegbusi and L. I. Trakhtenberg, *Sens. Actuators, B*, 2017, **240**, 613.
10 R. Godbole, V. P. Godbole and S. Bhagwat, *Mater. Sci. Semicond. Process.*, 2017, **63**, 212.
11 A. T. Mane, S. B. Kulkarni, S. T. Navale, A. A. Ghanwat, N. M. Shinde, J. H. Kim and V. B. Patil, *Ceram. Int.*, 2014, **40**, 16495.
12 B. T. Marquis and J. F. Vetelino, *Sens. Actuators, B*, 2001, **77**, 100.
13 N. Barsan and U. Weimar, *J. Electroceram.*, 2001, **7**, 143.
14 M. N. Rumyantseva, E. A. Makeeva, S. M. Badalyan, A. A. Zhukova and A. M. Gaskov, *Thin Solid Films*, 2009, **518**, 1283.
15 A. Gurlo, N. Bârsan and U. Weimar, in *Metal Oxides*, ed. J. L. G. Fierro, CRC Press, Boca Raton, 2006, pp. 683–738.
16 N. P. Zaretskiy, L. I. Menshikov and A. A. Vasiliev, *Sens. Actuators, B*, 2012, **170**, 148.
17 J. Tamaki, Z. Zhang, K. Fujimori, M. Akiyama, T. Harada, N. Miura and N. Yamazoe, *J. Electrochem. Soc.*, 1994, **141**, 2207.

Received: 14th June 2019; Com. 19/5953